Research Article | Vol. 29, No. 7 / 29 March 2021 / Optics Express 10491
Optics EXPRESS

Study of temporal, spectral, arrival time and energy fluctuations of SASE FEL pulses

IVETTE J. BERMÚDEZ MACIAS,[1] STEFAN DÜSTERER,[1,*] ROSEN IVANOV,[1] JIA LIU,[2] GÜNTER BRENNER,[1] JULIANE RÖNSCH-SCHULENBURG,[1] MARIE K. CZWALINNA,[1] AND MIKHAIL V. YURKOV[1]

[1]*Deutsches Elektronen-Synchrotron, Notkestrasse 85, D- 22603 Hamburg, Germany*
[2]*European XFEL GmbH, Holzkoppel 4, D- 22869 Schenefeld, Germany*
[*]*stefan.duesterer@desy.de*

Abstract: Self-amplified spontaneous emission (SASE) pulses delivered by free electron lasers (FELs) are inherently fluctuating sources; each pulse varies in energy, duration, arrival time and spectral shape. Therefore, there is strong demand for a full characterization of the properties of SASE radiation, which will facilitate more precise interpretation of the experimental data taken at SASE FELs. In this paper, we present an investigation into the fluctuations of pulse duration, spectral distribution, arrival time and pulse energy of SASE XUV pulses at FLASH, both on a shot-to-shot basis and on average over many pulses. With the aid of simulations, we derived scaling laws for these parameters and disentangled the statistical SASE fluctuations from accelerator-based fluctuations and measurement uncertainties.

1. Introduction

Free-electron lasers (FELs) working in the extreme ultraviolet (XUV) and X-ray region deliver photon pulses with few-femtosecond (fs) duration and unrivalled intensity [1–7]. The majority of X-ray FELs operate in the self-amplified spontaneous emission (SASE) regime, meaning that each pulse is characterized by a unique combination of pulse energy, XUV spectrum, arrival time and pulse duration (see e.g. Figure 1). For a detailed analysis of experimental data taken during FEL experiments it is essential to determine as many SASE pulse radiation properties as possible, at best on a shot-to-shot basis. A variety of pulse-resolved methods have been developed and are used to determine, e.g. the pulse energy [8,9], the spectral distribution [10,11] and arrival time of the electron bunches [12], but the XUV pulse duration still lacks a standard detection scheme. Providing accurate pulse length information would enable experimentalists to sort their experimental data according to all pulse properties. Furthermore, it would allow one to identify whether there are correlations between different parameters, such as pulse energy and duration. So far, many studies have examined the fluctuations in pulse energy [13–17] or XUV spectrum [17–21] separately. Due to the shortcomings of available pulse-resolved XUV pulse duration diagnostics, the influence of the SASE process on the temporal properties and the dependence of other parameters on the pulse duration have yet to be investigated in detail. In this paper, we present pulse-resolved measurements of the XUV pulse duration at the free-electron laser FLASH in Hamburg [1], achieved using THz streaking [22–24], in addition to measurements of the XUV spectrum and pulse energy of all individual pulses. The fluctuation of these parameters, as well as the correlations and dependencies between them are studied. Furthermore, simulations using a fast three dimensional, time-dependent simulation code FAST [25] and the partial coherence method [26], support our experimental findings and are used to disentangle the influence of the physics of the SASE process and its fluctuations from measurement uncertainties.

#419977 https://doi.org/10.1364/OE.419977
Journal © 2021 Received 21 Jan 2021; revised 26 Feb 2021; accepted 2 Mar 2021; published 18 Mar 2021

Optics EXPRESS

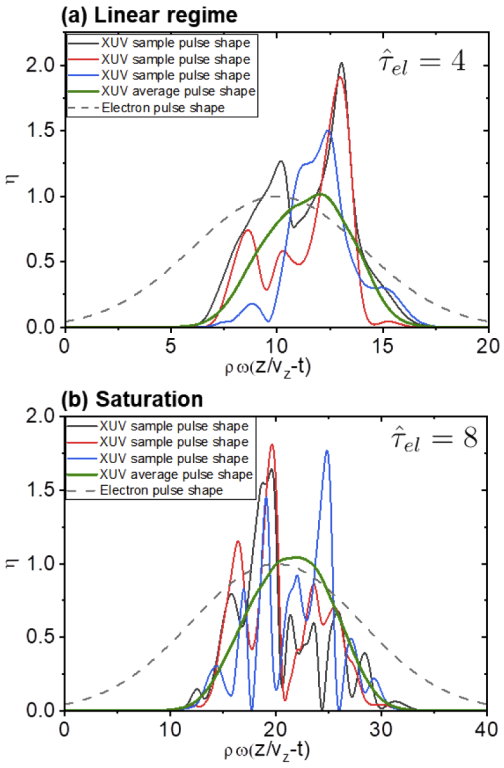

Fig. 1. The temporal distribution of a SASE pulse is illustrated with a simulation result using FAST. The x-axis, is the scaled time coordinate along the bunch where v_z is the longitudinal velocity of the electrons. Fig. (a) shows photon pulses generated in the linear regime ($\hat{\tau}_{\rm el} = 4$) and Fig. (b) at the onset of saturation ($\hat{\tau}_{\rm el} = 8$) . The dashed line denotes the electron bunch pulse shape.

A theoretical overview of the statistical properties of the SASE FEL radiation, as well as the methods and results of the numerical simulations, are presented in Sec 2. The experimental setup is described in Sec 3. In Sec 4 we discuss the experimental results and compare them to simulations. Furthermore, the average and shot-to-shot fluctuations of the FEL photon pulse duration, energy, and arrival time are presented in Sec 4.

2. Statistical properties of the SASE FEL radiation

The amplification process in a SASE FEL develops from the shot noise in the electron beam, and amplifies a narrow band of density modulations around the resonance wavelength $\lambda = \lambda_{\rm u}(1 + K^2)/(2\gamma^2)$. In the one-dimensional model's framework, the operation of a SASE FEL is described by the FEL parameter ρ and the number of cooperating electrons $N_{\rm c}$ [13,27] in the SASE process:

$$\rho = \left[\frac{\lambda_{\rm u}^2 j_0 K^2 A_{\rm JJ}^2}{16\pi I_A \gamma^3}\right]^{1/3}, \qquad N_{\rm c} = I/(e\rho\omega)\,, \tag{1}$$

where γ is the relativistic factor, j_0 is the beam current density, $I_A = mc^3/e \simeq 17$ kA, K is the rms undulator parameter, and $\lambda_{\rm u}$ is the undulator period. The coupling factor is $A_{\rm JJ} = 1$ for a helical undulator, and $A_{\rm JJ} = [J_0(Q) - J_1(Q)]$ with $Q = K^2/[2(1 + K^2)]$ for a planar undulator. I is the electron bunch current and ω the frequency of the amplified wave.

Optics EXPRESS

In this section, we assume that the electron bunch has a Gaussian longitudinal profile and its rms pulse duration is τ_{el}. We extend the results of Refs. [14,17] by in addition studying the statistical properties of the photon pulse duration and arrival time. We perform a series of numerical simulations of the FEL process using the simulation code FAST [25] for a wide range of electron bunch durations τ_{el}, and trace the FEL amplification process from the start-up of the shot noise to the deep nonlinear regime. Then, we apply similarity techniques [13] to the results of the numerical simulations and derive general statistical properties of the radiation.

The output of a specific simulation run is an array of radiation fields $\tilde{E}(t)$, from which we can calculate the temporal profile of the radiation power $P(t) \propto |\tilde{E}(t)|^2$ and the radiation pulse energy $E_{\mathrm{r}} = \int P(t)dt$ as shown in Fig. 1. The center of mass of the photon pulse, which we also associate with the photon pulse arrival time τ_{ar}, and its rms duration τ_{ph} are derived from numerical simulations as follows:

$$\tau_{\mathrm{ar}} = \frac{\int tP(t)\mathrm{d}t}{E_{\mathrm{r}}}\,, \qquad \tau_{\mathrm{ph}}^2 = \frac{\int (t-\tau_{\mathrm{ar}})^2 P(t)\mathrm{d}t}{E_{\mathrm{r}}}\,. \tag{2}$$

The energy, duration, and arrival time of the radiation pulses fluctuate from shot-to-shot. These fluctuations can be described with their standard deviations:

$$\begin{aligned} \sigma_{\mathrm{ph}}^2 &= \langle(\tau_{\mathrm{ph}} - \langle\tau_{\mathrm{ph}}\rangle)^2\rangle\,, \\ \sigma_{\mathrm{ar}}^2 &= \langle(\tau_{\mathrm{ar}} - \langle\tau_{\mathrm{ar}}\rangle)^2\rangle\,, \\ \sigma_{\mathrm{E}}^2 &= \langle(E_{\mathrm{r}} - \langle E_{\mathrm{r}}\rangle)^2\rangle/\langle E_{\mathrm{r}}\rangle^2\,. \end{aligned} \tag{3}$$

As a next step of the analysis, applying similarity techniques, we translate the results of a specific numerical simulation onto a map of physical parameters [13]. The typical temporal scaling factor in FEL physics is the coherence time τ_{c}, defined as $\tau_{\mathrm{c}} = \int |\gamma_c(t)|^2 dt$, with γ_c as the complex degree of coherence [28]. On the other hand, the relevant scaling parameter for the variables having a dimension of time is $\rho\omega$ leading to the following dimensionless expressions (the relation to experimental parameters can be found in Table 1):

$$\begin{aligned} \hat{\tau}_{\mathrm{el}} &= \rho\omega\tau_{\mathrm{el}}\,, & \hat{\tau}_{\mathrm{ph}} &= \rho\omega\tau_{\mathrm{ph}}\,, \\ \hat{\sigma}_{\mathrm{ar}} &= \rho\omega\sigma_{\mathrm{ar}}\,, & \hat{\sigma}_{\mathrm{ph}} &= \rho\omega\sigma_{\mathrm{ph}}\,. \end{aligned} \tag{4}$$

Table 1. The table shows the relation between normalized electron pulse durations $\hat{\tau}_{\mathrm{el}}$, that were used in the simulation and the corresponding expected XUV pulse durations in fs (FWHM) at the onset of saturation. Note that $\hat{\tau}_{\mathrm{el}}$ is equivalent to the number of modes M (for $\hat{\tau}_{\mathrm{el}}$>2). τ_{ph} was calculated according to Eq. (9). We used $\tau_{c_{FWHM}}$(6.8nm) ~ 6 fs and $\tau_{c_{FWHM}}$(20nm) ~ 15 fs (FWHM).

$\hat{\tau}_{\mathrm{el}}$ | M	$\tau_{\mathrm{ph,FWHM}}(6.8nm)$	$\tau_{\mathrm{ph,FWHM}}(20nm)$
4	17 fs	40 fs
8	35 fs	85 fs
16	70 fs	170 fs
32	140 fs	340 fs

Then scaling the parameters with the normalized electron pulse duration $\hat{\tau}_{\mathrm{el}}$, we obtain:

$$\begin{aligned} \bar{\tau}_{\mathrm{ph}} &= \tau_{\mathrm{ph}}/\tau_{\mathrm{el}}\,, & \bar{\sigma}_{\mathrm{ph}} &= \hat{\sigma}_{\mathrm{ph}}/\hat{\tau}_{\mathrm{el}}^{1/2}\,, \\ \bar{\sigma}_{\mathrm{ar}} &= \hat{\sigma}_{\mathrm{ar}}/\hat{\tau}_{\mathrm{el}}^{1/2}\,, & \bar{\sigma}_{\mathrm{E}} &= \sigma_{\mathrm{E}}\hat{\tau}_{\mathrm{el}}^{1/2}\,, \\ \bar{\eta} &= E_{\mathrm{r}}/(\rho \mathrm{E}_{\mathrm{eb}})\,, \end{aligned} \tag{5}$$

where E_{eb} is the kinetic energy of the electron bunch.

Optics EXPRESS

Figure 2 shows the evolution of the main characteristics of the SASE FEL electron and radiation pulse along the undulator. Using Eq. (5), the average values and fluctuations of the electron pulse energy and duration, as well as the arrival time of the radiation pulses' fluctuations, are shown. For radiation pulse durations $\hat{\tau}_{\rm el} \gtrsim 4$, the scaled parameters (5) show a common behavior. The longitudinal coordinate z along the undulator in Fig. 2 is scaled to the saturation length $z_{\rm sat}$ [13,29]:

$$z_{\rm sat} \simeq \frac{\lambda_{\rm u}}{4\pi\rho}\left(3+\frac{\ln N_{\rm c}}{\sqrt{3}}\right), \qquad \tau_{\rm c}^{\rm sat} \simeq \frac{1}{\rho\omega}\sqrt{\frac{\pi \ln N_{\rm c}}{18}}. \tag{6}$$

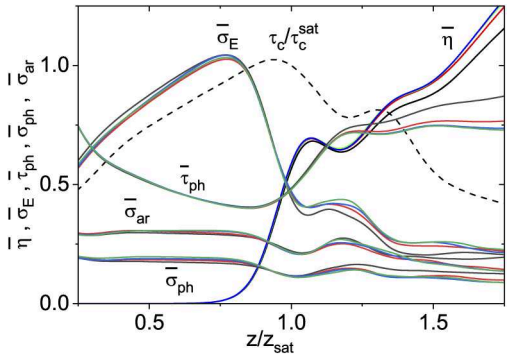

Fig. 2. Evolution along the undulator of the scaled FEL efficiency $\bar{\eta}$, scaled rms fluctuations of the radiation pulse energy $\bar{\sigma}_{\rm E}$, scaled rms photon pulse duration and its scaled rms deviation, $\bar{\tau}_{\rm ph}$ and $\bar{\sigma}_{\rm ph}$, as well as the scaled rms deviation of the photon pulse arrival time $\bar{\sigma}_{\rm ar}$. The notations of the scaled parameters are given by Eq. (5). The black, red, blue and green curves correspond to the normalized electron pulse durations $\hat{\tau}_{\rm el}$ of 4, 8, 16, and 32, respectively. The dashed line shows the coherence time scaled to the coherence time at saturation. The calculations are plotted as function of the undulator coordinate z normalized by the saturation length $z_{\rm sat}$. Thus, values $z/z_{\rm sat}$<0.8 denote the linear regime while $z/z_{\rm sat} = 1$ is the saturation point.

The brilliance of the radiation, which is proportional to the product of the radiation power and the coherence time, reaches a maximum value at the saturation point. The coherence time at the saturation point $\tau_{\rm c}^{\rm sat}$ is given by Eq. (6). It grows at a rate of $z^{1/2}$ in the exponential gain regime (also called linear regime), reaches a maximum value just before saturation, and gradually drops down in the post-saturation regime [13,30].

The maximum of the energy fluctuations and minimum of the radiation pulse duration are obtained at the end of the exponential gain regime, at about 0.8 of the saturation length. The radiation from a SASE FEL operating in the linear regime holds properties of completely chaotic polarized light [13,30], and the probability distribution of the radiation energy $E_{\rm r}$ is a gamma-distribution [30]:

$$p(E_{\rm r}) = \frac{M^M}{\Gamma(M)}\left(\frac{E_{\rm r}}{\langle E_{\rm r}\rangle}\right)^{M-1}\frac{1}{\langle E_{\rm r}\rangle}\exp\left(-M\frac{E_{\rm r}}{\langle E_{\rm r}\rangle}\right), \tag{7}$$

where $\Gamma(M)$ is the Gamma-function. The physical meaning of M is that it is equal to the total number of modes (longitudinal and transverse) in the radiation pulse. It is connected to the fluctuations of the radiation pulse energy by the relation $M = 1/\sigma_E^2$. Furthermore, at the onset of saturation, M essentially equals the normalized electron pulse duration $\hat{\tau}_{\rm el}$ (for M>2) as shown in Ref. [17].

The radiation of the SASE FEL at the initial stage of the amplification consists of a large number of transverse and longitudinal modes. The number of longitudinal modes is defined by

Optics EXPRESS

the fluctuations of the radiation pulse energy filtered with a pin hole, and it is improved along the amplification process, resulting in a reduction of the number of longitudinal modes. The transverse mode selection process leads to a suppression of the higher transverse radiation modes. As a result, primarily the fundamental transverse mode dominates in the high-gain linear regime for diffraction-limited electron beams. This feature makes the one-dimensional model applicable for the description of FELs like FLASH.

A practical estimate for the minimum rms radiation pulse duration at the end of the high-gain linear regime is [16,17]:

$$\tau_{\mathrm{ph}}^{\mathrm{min}} \simeq 0.4\tau_{\mathrm{el}} \simeq \frac{M\lambda z_{\mathrm{sat}}}{15c\lambda_{\mathrm{u}}} \simeq \frac{M\tau_{\mathrm{c}}^{\mathrm{sat}}}{4}\,. \tag{8}$$

The lengthening of the radiation pulse occurs when the amplification process enters the nonlinear regime. This happens due to the electron bunch tails lasing into saturation and the slippage effect. The latter is more pronounced for shorter pulses, as illustrated in Fig. 2. At the saturation point, the lengthening is about a factor of 1.2 greater with respect to the minimum pulse length given by Eq. (8), and it increases up to a factor of 1.8 in the post-saturation regime. To compare these results to the experimentally determined data, a scaling of Eq. (8) to full width half maximum (FWHM) is helpful:

$$\tau_{\mathrm{ph_{FWHM}}}^{\mathrm{sat}} \simeq 0.7M\tau_{\mathrm{c_{FWHM}}}^{\mathrm{sat}} \tag{9}$$

using the experimentally easier accessible FWHM of the coherence time which is linked to $\tau_{\mathrm{c}}^{\mathrm{sat}}$ by $\tau_{\mathrm{c_{FWHM}}}^{\mathrm{sat}} = 2\sqrt{\ln 2/\pi} \times \tau_{\mathrm{c}}^{\mathrm{sat}} \sim 0.94 \times \tau_{\mathrm{c}}^{\mathrm{sat}}$ [28].

In addition, the relation between the number of spikes (N_{spect}) present in the spectral distribution and the number of modes is important for the analysis of the experimental data. Following the argumentation in Ref. [31] we obtain the relation:

$$N_{\mathrm{spect}} \sim 0.7M. \tag{10}$$

Looking at Fig. 3 the following scaling of the pulse duration fluctuation can be deduced:

$$\frac{\sigma_{\mathrm{ph}}}{\tau_{\mathrm{ph}}} \simeq \frac{\alpha_{\mathrm{ph}}}{\sqrt{\hat{\tau}_{\mathrm{el}}}} \simeq \frac{\alpha_{\mathrm{ph}}}{\sqrt{M}} \tag{11}$$

with the scaling parameter α_{ph} ranging between 0.4 for the linear regime and 0.2 in saturation. Equivalently, for the pulse arrival time fluctuation we obtain:

$$\frac{\sigma_{\mathrm{ar}}}{\tau_{\mathrm{ph}}} \simeq \frac{\alpha_{\mathrm{ar}}}{\sqrt{\hat{\tau}_{\mathrm{el}}}} \simeq \frac{\alpha_{\mathrm{ar}}}{\sqrt{M}} \tag{12}$$

with $\alpha_{\mathrm{ar}} \sim 0.7$ for the linear regime and $\alpha_{\mathrm{ar}} \sim 0.4$ in saturation.

The ratio $\sigma_{\mathrm{ph}}/\sigma_{\mathrm{ar}} \simeq 0.6$ remains nearly constant for all the stages of the amplification process. Thus, the SASE induced fluctuation of the arrival time (movement of the centroid) is about twice as large compared to the fluctuations of the pulse duration itself. This has important consequences for high precision pump-probe experiments where the arrival time of the applied pulses has to be known precisely.

Figure 4 shows the correlation plots of the photon pulse duration versus the radiation pulse energy for several thousand simulation runs. A clear correlation is visible in the high-gain linear regime where *shorter* pulses contain *more* energy while for saturation and post-saturation there is no significant correlation as will be discussed in the next section.

In addition to the advanced simulation of the actual SASE process, a very simple but powerful approach based on the *partial coherence model* introduced in Ref. [26] was used to determine to what extent this model agrees with the experiments. This method generates a random spectral

Optics EXPRESS

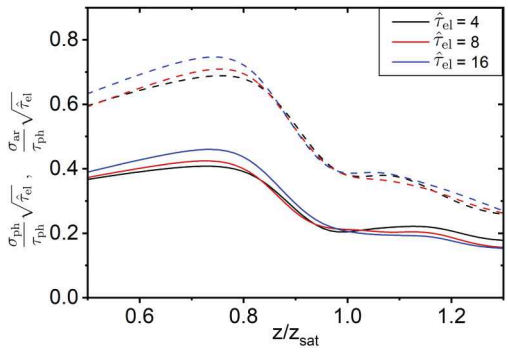

Fig. 3. Shown is the evolution of the fluctuations normalized on the pulse duration for the pulse arrival time $\sigma_{ar}/<\tau_{ph}>$ and pulse duration $\sigma_{ph}/<\tau_{ph}>$ scaled with the normalized electron pulse duration $\sqrt{\hat{\tau}_{el}}$. The plot reflects how the fluctuations decrease as saturation is reached. Pulse arrival time fluctuations dominate over the pulse duration fluctuations. The three different colors of the curves correspond to the different normalized electron pulse durations $\hat{\tau}_{el}$ = 4, 8 and 16.

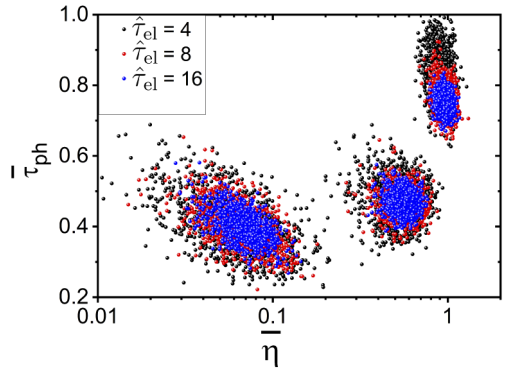

Fig. 4. Correlation plot of the scaled rms photon pulse duration $\bar{\tau}_{ph}$ versus the scaled photon pulse energy $\bar{\eta}$. Black, red and blue colors correspond to the normalized electron pulse durations $\hat{\tau}_{el}$ = 4, 8 and 16. The left area of the plot corresponds to the high-gain linear regime ($z = 0.8 \times z_{sat}$), where a negative slope can be observed predicting shorter pulses at larger pulse energies. The middle and right areas correspond to the saturation, and deep nonlinear regime ($z = 1.5 \times z_{sat}$), where no correlation is found (compare with Fig. 2). The notations of scaled parameters are given by Eq. (5).

phase and amplitude distribution at different sample frequencies which are used to create an initial electric field. This field is "filtered" with the (measured) average spectral distribution of the FEL. After a Fourier transform, this leads to a series of coherent spikes in the time domain, which, in a second step, is folded with the desired average pulse duration shape, restricting the electric field to the finite pulse duration. This step finally leads to the characteristic spectral spikes after a second Fourier transform back to the spectral domain. The new filtered electric field will be partially coherent as it is delimited by the known FEL pulse duration and average spectrum and will be different for each random choice of the spectral phase function. Using this approach, one can easily provide a large set of simulated SASE-like pulse distributions to model SASE FEL experiments.

Optics EXPRESS

3. Description of experiment

The experiments were performed at the plane grating (PG) beamline [32] of FLASH. For the experiments described here, the PG beamline was operated in so called parallel configuration. This special mode enables the utilization of the zero order of the FEL photon beam (at the PG0 beamline branch) for the pulse length diagnostic based on THz streaking [24], while the dispersed radiation is simultaneously used in the PG2 beamline to measure the FEL spectrum with high resolution [33]. This configuration was used for the presented measurement in order to acquire the maximum amount of information about the XUV SASE pulses.

Various settings of the accelerator were used to provide a large range of different radiation pulse properties. The electron bunch charges were altered from 0.08 nC up to 0.44 nC leading to different XUV pulse durations as well as to XUV pulse energies ranging between only few μJ to > 100 μJ per XUV pulse. FLASH was tuned to a wavelength of 6.8 nm (180 eV) and for a second set of measurements to 20 nm (62 eV).

The FEL was operated in single bunch mode at 10 Hz. To generate single-cycle THz pulses, the near-infrared (NIR) pump-probe laser system at FLASH [34] was used. This Ti:sapphire laser delivers ~100 fs (FWHM) pulses with 6.5 mJ pulse energy at a central wavelength of 800 nm and a repetition frequency of 10 Hz. The overall level of synchronisation between the NIR pulses and the XUV FEL pulses was on the order of few tens of fs jitter (FWHM) (for the description of the synchronization system see e.g. [35]). The THz streaking setup consists of an optical setup with beam size adaption, pulse front tilting, THz generation and transport to the interaction region as well as an UHV interaction chamber. An electron time-of-flight (TOF) with high collection efficiency (Kaesdorf ETF11) mounted on a 3D manipulator records the time-of-flight of photoelectrons upon XUV ionization of the rare gas atoms target. A detailed description of the setup and measurement procedures are presented in Refs. [24,36].

Using the current THz streaking setup it was not possible to resolve the pulse sub structure, e.g the individual longitudinal modes of the pulse. The instrument broadening resulted in a Gaussian photoelectron distribution. The measured photoelectron line was therefore fitted using a Gaussian distribution.

The streaking measurements are rather complex and thus the measurement uncertainty depends on various parameters, which are described in detail in [36]. Generally, an error bar of ± 20% is in good agreement with the detailed investigations.

In addition to the XUV pulse duration and the XUV spectrum, the shot-to-shot pulse energy was recorded simultaneously using a transparent pulse energy monitor [8,9] located upstream of the THz-streaking setup and the PG beamline as well as the electron bunch arrival time [12].

4. Results and discussion - Characterization of SASE radiation

FLASH is a very versatile free-electron laser, able to deliver radiation across a wide range of wavelengths and pulse durations. Using these opportunities we could experimentally determine dependencies between XUV pulse duration, XUV spectral distribution and XUV pulse energy for many thousands of pulses and different machine settings, as will be shown in this section.

4.1. Fluctuations of the radiation pulse duration

The single-shot SASE XUV pulse duration derived from the THz streaking measurements reveals large fluctuations from shot-to-shot as shown in Fig. 5(a). The pulse duration from one pulse to the next can change by a factor of two to three. Likewise, the pulse energy and arrival time show strong fluctuations as presented in Fig. 5(b). These are the fluctuations experiments must cope with in the course of analyzing and interpreting the measured data. In addition, Fig. 5 emphasizes the need for an online pulse-resolved photon diagnostic of the radiation parameters at SASE FELs. An interesting question arises: What is the actual source of the fluctuations -

Optics EXPRESS

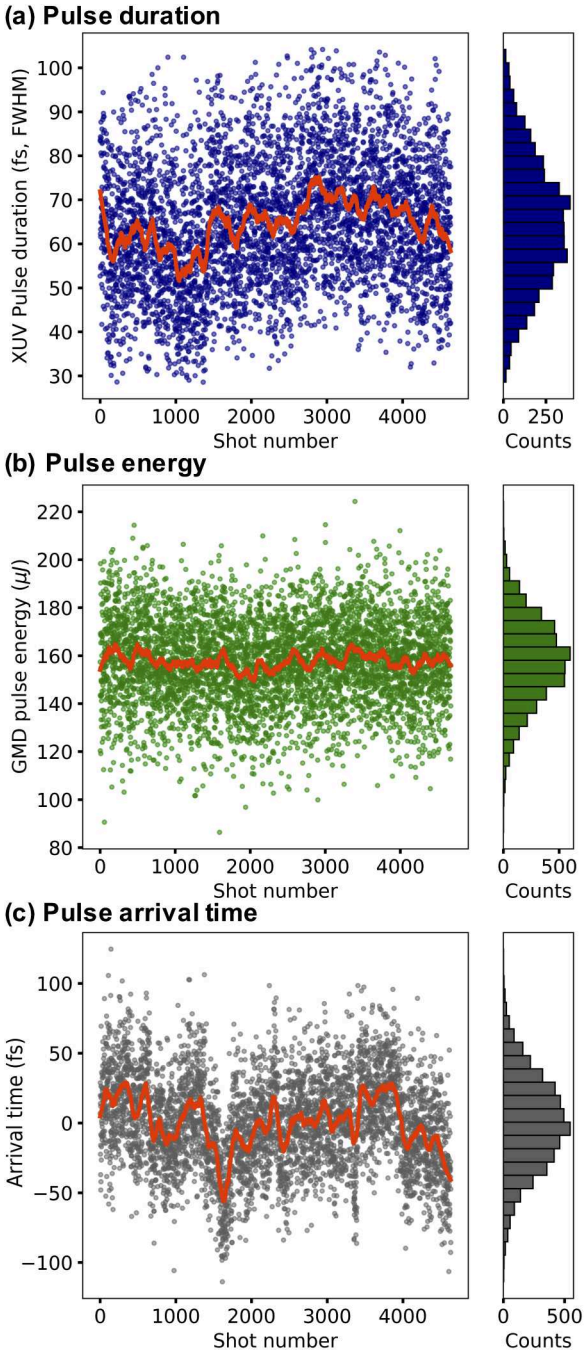

Fig. 5. The plots show how the measured XUV pulse duration (a), energy (b) and arrival time (c) fluctuate from pulse to pulse for around four thousand FLASH pulses. The line indicates the mean value. Error bars (not shown) are on the order of 20 % for the pulse duration and <10% for the pulse energy measurements. The arrival time uncertainty measured by THz streaking was ~ 20 fs. In addition, the histograms of the shown time series are shown.

Optics EXPRESS

SASE or technical fluctuations? To get information on the fluctuations source, simulations of the different FEL parameters that are only taking the SASE process into account are used to compare to the experimentally determined values. That way we can disentangle the fluctuations induced by inherent SASE fluctuations from measurement uncertainties, fluctuations in the energy gain and compression of the electron bunches (related to the acceleration field phase stability), that we summarize and refer to as "technical fluctuations".

As shown in Fig. 5 (a, right side), the histogram of the measured pulse durations has a Gaussian distribution, with its center of mass denoting the mean pulse duration width representing the shot-to-shot fluctuations. To compare the width of the distribution for different pulse duration settings of the FEL, we use the rms of the distribution normalized by the pulse duration (σ_{ph}/τ_{ph}).

Equation (11) shows that the relative fluctuations of the pulse duration depend on the number of spectral modes. Therefore, in order to compare the experimental values measured at 6.8 nm , 20 nm and the simulation, the measured pulse duration was converted to the number of modes using Eq. (9). The coherence times τ_c were taken from Ref. [37]: $\tau_{c_{FWHM}}$(6.8 nm)~ 6 fs and $\tau_{c_{FWHM}}$(20 nm)~ 15 fs as summarized in Table 1.

The relative pulse duration fluctuations determined by the THz streaking experiments are plotted in Fig. 6 (dots) together with the simulation results [Eq. (11)] for saturation (full line) and exponential gain regime (dashed line). The experimental data points are the average fluctuations for several thousand FEL pulses recorded for different FEL operation modes. The fluctuation decreases when increasing the pulse duration from (σ_{ph}/τ_{ph}) ~ 30% for short pulses to ~ 10% for longer ones. Therefore, SASE delivers better defined pulse durations for longer pulses than for short pulses. The general trend can be understood by looking at the modal structure; short pulses consist only of a small number of modes/spikes, such that the relative change of ±1 modes affect the pulse duration much stronger than for longer pulses consisting of many more modes.

Comparing the measured data with the predicted pure SASE fluctuations from the FAST simulation (see Fig. 6), we find that a large fraction of the fluctuations is due to the SASE process. However, 20-50 % of the fluctuations can be attributed to "technical sources". Since the FEL was operating close to or in saturation, the relevant simulation for comparison is that of the solid line. The error bars include the uncertainty of the single-shot pulse duration measurement as described in [36] but accelerator based fluctuations are not taken into account.

The identification and quantification of other sources of fluctuations will have to be addressed in future studies. Even if additional "technical" error sources will be minimized in future accelerators, the pulse duration fluctuations based on pure SASE are still significant. Looking at Fig. 1 the pulse shape and resulting intensity distribution changes much more from shot-to-shot than the rms width, which underlines the demand for a high resolution temporal diagnostic resolving the SASE substructure.

In order to test to what extent the partial coherence model simulation [26] can reproduce the predicted fluctuations, we generated a large set of XUV spectra and temporal distributions. Ensembles of 400 pulses were calculated for different pulse durations between 10 fs and 200 fs in combination with a range of spectral bandwidths from 0.2 % to 0.9 %. For each simulated pulse we derived the pulse duration using Eq. (2) and its number of modes by counting the spectral spikes and using Eq. (10). For each setting, the standard deviation over the 400 pulses was calculated and normalized by the average pulse duration. The result is plotted in Fig. 6 as orange diamonds. Despite the large variation of input parameters, the simulated fluctuations agree very well with the fluctuations for pulses at saturation as predicted by the FAST simulation. Since FLASH typically operates in saturation, we can conclude that the partial coherence model provides a simple scheme to simulate SASE pulses that resemble the theoretically expected scaling of the pulse duration fluctuations.

Optics EXPRESS

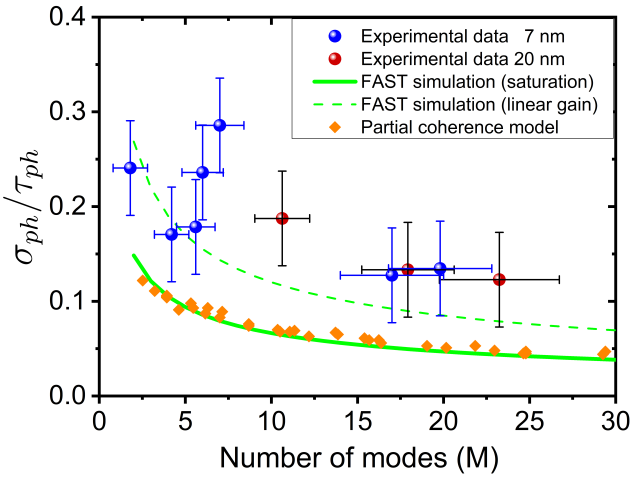

Fig. 6. The relative fluctuation of the SASE pulse durations are shown for the FAST simulation results as well as the experimentally measured values. The experimental pulse durations (for 6.8 nm and 20 nm) were scaled to number of modes using Eq. (9). The expected scaling of the fluctuations [(see Fig. 3 and Eq. (11)] are shown for the linear range and at saturation. In general, the relative fluctuations are decreasing for longer pulse durations while the experimental values (measured at saturation conditions) exceeding the simulation values indicating a significant contribution by technical fluctuations and drifts in the accelerator and measurement uncertainties of the THz streaking. In addition, the normalized fluctuations of 400 simulated pulses, calculated using the partial coherence method [26] are plotted.

4.2. *Fluctuations of the radiation pulse energy*

The pulse energy fluctuations can be treated analogously to the pulse duration fluctuations. As indicated in Fig. 2, the (relative) pulse energy fluctuations are larger compared to the pulse duration fluctuations and the difference between the linear gain and saturation regime is bigger as well.

Figure 7 summarizes the simulation results and the experimental data points. The experimental data lies between the predicted curves for the linear and the saturation regime. The pulse energy fluctuations of the experimental data are closer to the simulated ones, which is partly due to the much lower measurement uncertainty of typically $\pm(5-10)\%$ for pulse energy measurements [8,9]. Nevertheless, similar to the pulse duration fluctuations, a significant fraction of the fluctuations can be assigned to technical sources. Again, the partial coherence model agrees well with the FAST simulation for the saturation regime.

4.3. *Fluctuations of the arrival time*

Due to the varying sub-structure of the XUV pulse, the center of mass of the photon pulse (τ_{ar}) is slightly different from pulse to pulse, leading to fluctuations in the arrival time σ_{ar} of the photon pulse with respect to the electron bunch. To compare the prediction to the experimentally determined values we can use the arrival time of the center of mass of the electron bunch with respect to the master optical clock, which is measured at FLASH with high accuracy ($\sim$ 10 fs rms [12,35]) by the so called bunch arrival time monitor (BAM). In addition, the THz streaking arrival time measurements of the center of mass of the XUV photon pulse with respect to the THz pulse is monitored with few fs resolution [35]. However, after accounting for the synchronization

Optics EXPRESS

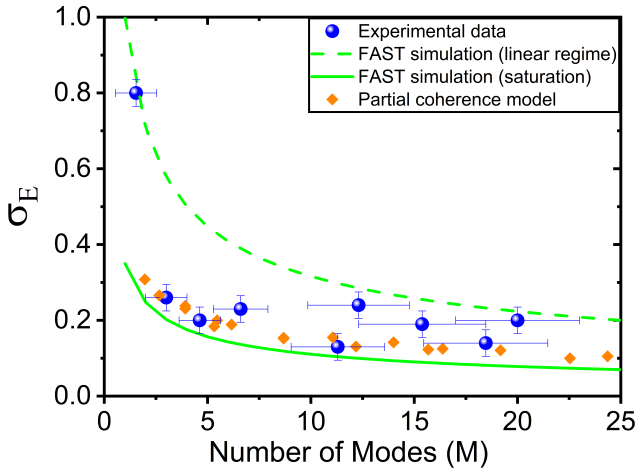

Fig. 7. The relative fluctuation of the SASE pulse energy is shown for the FAST simulation results as well as the experimentally measured values. The experimental pulse energy was measured for different FEL operation modes, from few μJ to up to 50 μJ. The simulated fluctuations are shown for the linear range and at saturation. In general, the relative fluctuations decrese for longer pulse durations. The experimental values (measured at saturation conditions) exceed the simulation values, indicating a significant contribution of technical fluctuations and drifts in the accelerator and measurement uncertainties.

of the THz producing laser to the master optical clock, the distribution of synchronised optical clock signals, transport of the electron bunches and XUV radiation by many tens of meters, as well as several other involved subsystems, the overall accuracy of arrival time determination between the electron bunch and the XUV photon pulse measured with THz streaking is in the range of 15-20 fs rms (corresponding to 30-50 fs FWHM) [24].Looking at the theoretical prediction of SASE arrival time fluctuations [Eq. (12)] we find, for the presented parameter range of wavelengths and pulse durations, that the arrival time fluctuations due to the statistical variation of the photon pulse sub-structure are below 10 fs (rms) and thus can not be determined using current arrival time measurement techniques. Figure 8 shows the relative fluctuations of the arrival time simulated using FAST for the linear and non-linear regime and the partial coherence model. The experimental arrival time fluctuations were calculated by taking the standard deviation of the difference between the photon arrival time measured by THz streaking (τ_{ph}) and the electron beam arrival time (τ_{BAM}). The 15-20 fs rms accuracy of the photon pulse arrival time measurements is much larger as compared to the pulse duration, therefore the relative fluctuations are greater and it is used as the upper limit of the fluctuation's uncertainty.

4.4. Correlations of the radiation pulse energy and pulse duration

In the previous sections, fluctuations of pulse energy and pulse duration were discussed as average values and independently from each other. With thousands of experimental and simulated pulse durations and corresponding pulse energies of individual SASE pulses, the analysis can be extended to a shot to shot basis.

Studying the temporal structure of the SASE pulses (Fig. 1), one is tempted to conclude that a longer pulse containing more sub spikes (modes) also contains more photons on average and thus has a higher pulse energy. Plotting the single-shot normalized pulse duration and corresponding pulse energies for different FEL settings, we obtain the correlation plots shown in Fig. 9(a). Three different FEL settings were used, with ~17 fs, ~35 fs and ~70 fs (FWHM)

Optics EXPRESS

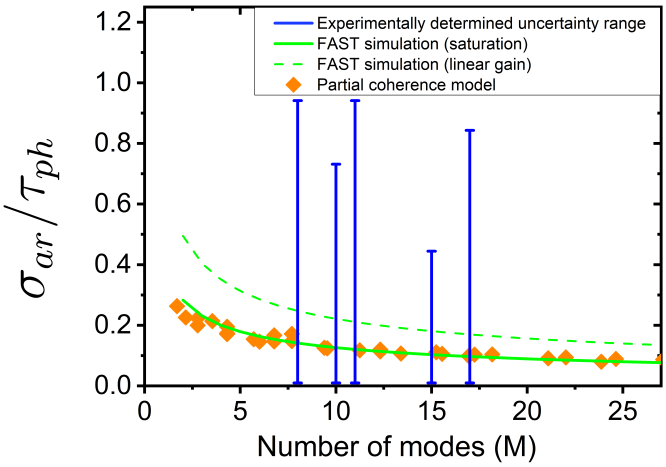

Fig. 8. The relative fluctuation of the SASE arrival time using the FAST and partial coherence model simulations are shown. The fluctuations were calculated for the saturation (solid line) and linear (dashed line) regime. The arrival time fluctuations simulations decrease for longer pulse durations. The current experimental resolution of 15-20 fs gives an upper limit on the uncertainty of the measured arrival time relative fluctuations.

average pulse durations [converted to the number of modes by Eq. (9)]. Firstly, the fluctuations are not correlated for any of the measured FEL settings. Thus, perhaps surprisingly, the pulse energy fluctuates independently of the pulse duration, contradicting the simple interpretation mentioned above. Furthermore, the normalized fluctuations show about the same amplitude for the pulse energy and the pulse duration. In addition, there are smaller fluctuations for longer pulses, containing more modes. These observations are in agreement with the averaged data shown in Figs. 6 and 7. The error bars of a single shot measurement are shown in the lower right edge of Fig. 9(a) - the relatively large uncertainty may obscure any possible correlation. Simulations can help to clarify this situation.The simulation results calculated by FAST are plotted in Fig. 9(b). There is also no sign of correlation between pulse duration and pulse energy, supporting the experimental finding. We therefore conclude that the pulse energy and pulse duration are indeed fluctuating independently. Similar to the experiment, the simulated data shows smaller fluctuations in both quantities for longer pulses (larger number of modes). However, in contrast to the experimental values, the fluctuations for the pulse durations are smaller than those in pulse energy, in agreement with Fig. 2. The simulated pulse duration values fluctuate less in comparison to the experimental ones.

Despite the surprising result that there is no significant correlation between the pulse energy and the pulse duration of individual SASE pulses, there is an even more surprising observation obtained from the simulation for the linear gain regime. Figure 4 displays the pulse resolved correlation plots for the pulse duration and pulse energy at different stages along the undulator. When moving from the linear regime to deep saturation, the pulse energy increases by approximately two orders of magnitude, and the pulse duration increases by a factor of approximately two. While there is no correlation found in saturation, there is a tilted ellipse for the linear regime (Fig. 4), indicating a negative correlation between pulse energy and pulse duration. On average, pulses with shorter pulse duration actually contain *more* pulse energy. One possible explanation would be the following: Slightly increased intensity spikes in the initial random "seed" distribution gain faster more energy due to the exponential growth, leading to strong spikes. In contrast,

Optics EXPRESS

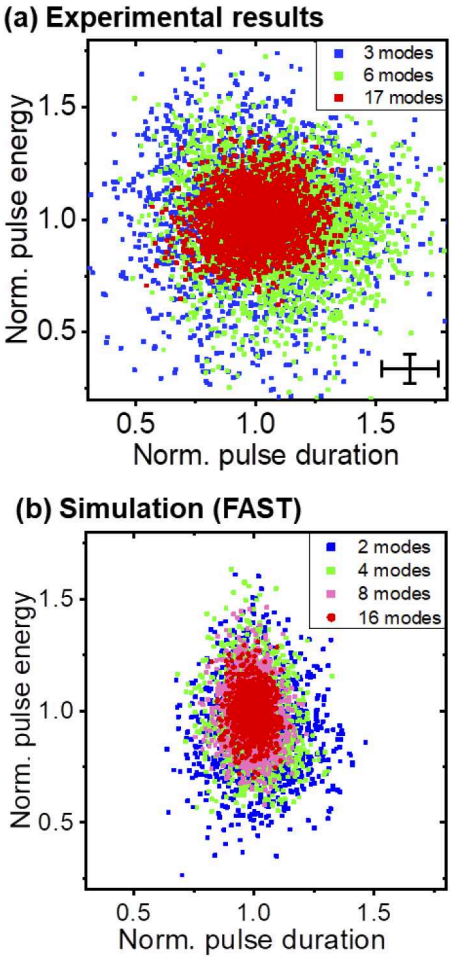

Fig. 9. Normalized and pulse resolved SASE pulse energy versus radiation pulse duration in the saturation regime. The experimental data (a) results from three different FEL settings at 6.8 nm with average pulse durations of ~15 fs, ~30 fs and ~90 fs (FWHM). The error bars for the single pulse measurements are shown in the lower right corner. Part (b) shows the simulation result (FAST) for different number of modes at saturation ($z/z_{\mathrm{sat}} = 1$). The fluctuations of the pulse energy are (for the same number of modes) about a factor of 2 larger as compared to the pulse duration in accordance to Fig. 2. The difference to the experimental result can be explained by measurement uncertainties and accelerator fluctuations.

the less intense parts of the initial distribution gain less energy and catch up only at saturation. Therefore, in the exponential gain regime, single intense spikes are more strongly amplified, leading to a larger fraction of short and intense pulses in the correlation plot. This results in an anti-correlation between pulse energy and pulse duration. Up to now the experimental resolution for pulse duration measurements at very low pulse energies has been insufficient to determine this negative correlation in the linear regime.

4.5. Radiation pulse duration and spectral structure

Generally, the spectral distribution of SASE XUV pulses also contains important information about the pulse duration. The second order spectral correlation function (g_2) [19–21] is typically

Optics EXPRESS

used to determine average pulse duration estimates from spectral information using the width of the spectral spikes. In Ref. [24] it is also demonstrated that there is a good agreement between XUV pulse durations determined by THz streaking and the g_2 method. However, a more experimentally straightforward method is to simply count the number of spectral spikes, which is a widely used technique that has not been investigated in detail so far.

As introduced in Eq. (8), the SASE pulse duration depends linearly on the number of modes. Strictly speaking, this relation only holds for the *linear gain regime* below saturation and it is a statistical parameter for average values calculated from an ensemble of data [19,31]. The extent to which this simple relation can be used as quick online analysis to estimate the pulse duration in saturation was investigated experimentally.

Figure 10 displays the FEL spectra measured as described in section 3, for different pulse lengths. The number of spectral modes was determined by a peak detection algorithm using a threshold of 20% of the maximum peak and a minimum distance between spikes. It was carefully checked that the counted number of peaks did not depend on the exact settings of the algorithm. However, considering that there may be overlapping modes which are not detected as two separated peaks, the number modes determined may underestimate the actual number of modes.

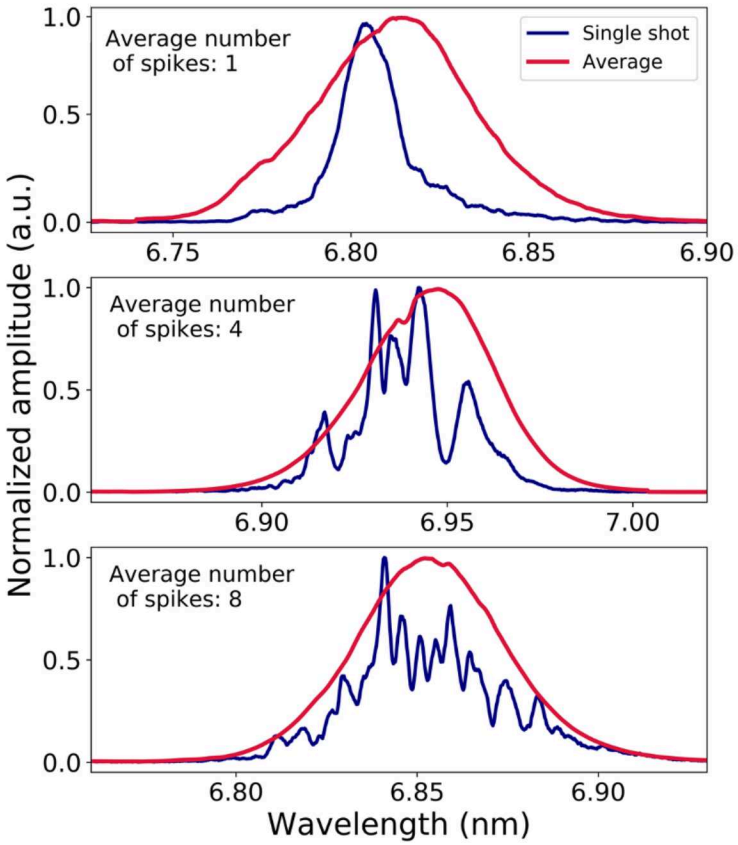

Fig. 10. FEL spectra measured at the PG2 beamline [32] for different pulse lengths. The blue line represents a single spectrum and the red line, the average over thousands of pulses. One can see the spiky nature of the SASE pulses in the spectral domain. The measurements show an increasing number of spikes for longer pulse durations.

Optics EXPRESS

Since the XUV spectra and the streaking measurements are acquired simultaneously, we can determine the number of spikes and the pulse duration for each recorded FEL setting. Figure 11 shows the averaged pulse duration and number of spectral spikes for different electron bunch length settings at FLASH. For most of the settings the FEL was operated in saturation, delivering over 15 μJ per XUV pulse. The measured relation between spectral modes and XUV pulse duration can be well approximated with a linear slope -as expected for the linear gain regime- even though already operating in saturation. The slope was determined to be 6.5 fs/spike, yielding a coherence time of ~ 6.5 fs (FWHM) for 6.8 nm [see Eqs. (9) and (10)], which is in good agreement with longitudinal interference measurements presented in Ref. [37]. Figure 11 shows the linear dependence between the *averaged* values of the number of spikes in the spectral domain and the pulse duration measured with streaking.

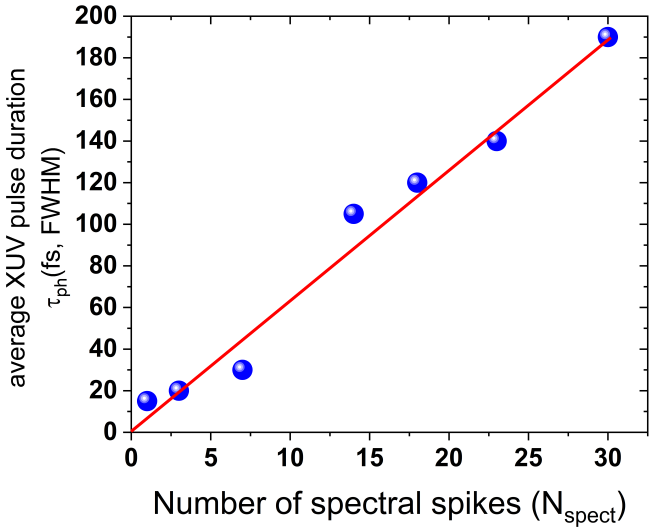

Fig. 11. Plotted is the experimentally determined average pulse duration as function of the average number of spectral spikes for different FEL operation settings (all at a wavelength of 6.8 nm). Several thousand pulse resolved measurements have been averaged for each data point. The FEL was operated close to or in saturation. The linear fit shows 6.5 fs/spectral spike.

To investigate the correlation for single SASE pulses, the number of spikes and the pulse duration are plotted for each SASE pulse in Fig. 12(a). Plotting the data for a fixed FEL setting, there is almost no correlation between the single-shot spike number and the pulse duration. For the same number of spikes, there can be up to a factor of two difference in pulse duration which does not allow one to predict, on a single shot basis, the XUV pulse duration from the spectral measurements. This experimental finding, shown in Fig. 12(a), is also confirmed by simulations. Using the partial coherence model [26], SASE pulses in temporal and spectral domain, were calculated for different average pulse durations and analyzed with the same peak finding algorithm as the experimental data. Similar to the experimental data there is a large scatter observed within the simulation results belonging to the same average pulse duration [Fig. 12(b)].

While there is on *average* and in saturation, a linear dependence between the pulse duration and the number of spectral spikes in the SASE radiation, both quantities fluctuate independently on a single-shot basis.

Optics EXPRESS

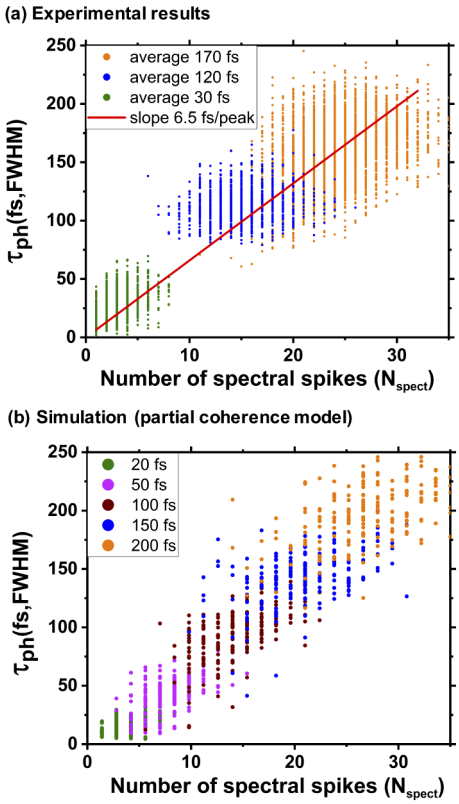

Fig. 12. Shown is the pulse resolved correlation between the number of spectral spikes and the pulse durations. The experimentally determined data was recorded for three different operation modes of the FEL with average pulse durations of 30fs, 120fs and 170 fs (at 6.8 nm). For a fixed FEL operation mode the pulse duration and number of spectral spikes fluctuate independently. This observation is supported by simulation results (b). Using the partial coherence method [26] the same behavior was observed.

5. Conclusion

We presented experimental data from the XUV SASE FEL FLASH for pulse duration, pulse energy, arrival time and spectral distribution. The fluctuations of these four important radiation pulse properties have been investigated on average and on a pulse to pulse basis for FEL pulses ranging from a few fs to up to 200 fs (FWHM). SASE simulations have been performed to support the experimental results and to disentangle experimental fluctuations and uncertainties from pure SASE related fluctuations. This approach shows that the major contribution of fluctuation is indeed caused by SASE, accompanied by a varying part of "technical" fluctuations. Analyzing the simulation results, scaling laws for the fluctuations have been derived theoretically and validated experimentally. The resulting $1/\sqrt{M}$ scaling allows a fast and precise way to estimate the amount of fluctuations of SASE parameters to expect for different FEL pulse durations and wavelengths without the need to perform complex simulations. Recording spectral and temporal pulse properties simultaneously for a large number of different FEL settings, we could experimentally verify that the linear dependence between the *average* pulse duration and *average* number of spectral spikes which was expected for the linear range by theory, still holds when the FEL is operated in saturation. This linear dependence however, disappears completely when the data is analyzed on a shot-to-shot basis. We found no correlation between single-shot pulse duration and

Optics EXPRESS

number of spectral spikes as well as pulse energy - all three parameters fluctuate independently in the experiment and the simulations. This result shows clearly that dependencies that were observed for averaged parameters may not hold for SASE based shot-to-shot fluctuations. This is important for FEL photon diagnostics, pointing out that one can *not* simply employ one quantity to predict the other on a shot-to-shot basis. It is not possible to substitute a complex task such as measuring the XUV pulse duration by just measuring the spectrum or even pulse energy. On the other hand, the missing correlation between the different radiation parameters is good news for the analysis of experimental data since it allows to sort the experimental data independently by one of the parameters without the risk to generate spurious correlations by the sorting procedure.

Acknowledgments. We want to acknowledge the work of the scientific and technical team at FLASH. We want to thank M. Beye and C. Passow for the implementation of the partial coherence model in Python.

Disclosures. The authors declare no conflicts of interest.

References

1. W. Ackermann, *et al.*, "Operation of a free-electron laser from the extreme ultraviolet to the water window," Nat. Photonics **1**(6), 336–342 (2007).
2. P. Emma, *et al.*, "First lasing and operation of an ångstrom-wavelength free-electron laser," Nat. Photonics **4**(9), 641–647 (2010).
3. T. Ishikawa, *et al.*, "A compact x-ray free-electron laser emitting in the sub-ångström region," Nat. Photonics **6**(8), 540–544 (2012).
4. E. Allaria, *et al.*, "Highly coherent and stable pulses from the fermi seeded free-electron laser in the extreme ultraviolet," Nat. Photonics **6**(10), 699–704 (2012).
5. W. Decking, *et al.*, "A mhz-repetition-rate hard x-ray free-electron laser driven by a superconducting linear accelerator," Nat. Photonics **14**(6), 391–397 (2020).
6. I. Ko, *et al.*, "Construction and commissioning of pal-xfel facility," Appl. Sci. **7**(5), 479 (2017).
7. C. Milne, *et al.*, "Swissfel: The swiss x-ray free electron laser," Appl. Sci. **7**(7), 720 (2017).
8. M. Richter, "Measurement of gigawatt radiation pulses from a vacuum and extreme ultraviolet free-electron laser," Appl. Phys. Lett. **83**(14), 2970–2972 (2003).
9. K. Tiedtke, J. Feldhaus, U. Hahn, U. Jastrow, T. Nunez, T. Tschentscher, S. V. Bobashev, A. A. Sorokin, J. B. Hastings, S. Möller, L. Cibik, A. Gottwald, A. Hoehl, U. Kroth, M. Krumrey, H. Schöppe, G. Ulm, and M. Richter, "Gas detectors for x-ray lasers," J. Appl. Phys. **103**(9), 094511 (2008).
10. G. Brenner, S. Kapitzki, M. Kuhlmann, E. Ploenjes, T. Noll, F. Siewert, R. Treusch, K. Tiedtke, R. Reininger, M. D. Roper, M. A. Bowler, F. M. Quinn, and J. Feldhaus, "First results from the online variable line spacing grating spectrometer at flash," Nucl. Instrum. Methods Phys. Res., Sect. A **635**(1), S99–S103 (2011).
11. M. Braune, G. Brenner, S. Dziarzhytski, P. Juranic, A. Sorokin, and K. Tiedtke, "A non-invasive online photoionization spectrometer for flash2," J. Synchrotron Radiat. **23**(1), 10–20 (2016).
12. A. Angelovski, M. Kuntzsch, M. K. Czwalinna, A. Penirschke, M. Hansli, C. Sydlo, V. Arsov, S. Hunziker, H. Schlarb, M. Gensch, V. Schlott, T. Weiland, and R. Jakoby, "Evaluation of the cone-shaped pickup performance for low charge sub-10 fs arrival-time measurements at free electron laser facilities," Phys. Rev. Spec. Top.–Accel. Beams **18**(1), 012801 (2015).
13. E. Saldin, E. Schneidmiller, and M. Yurkov, *The Physics of Free Electron Lasers* (Springer, 2000).
14. E. Saldin, E. Schneidmiller, and M. Yurkov, "Statistical properties of radiation from sase fel driven by short electron bunches," *Nuclear Instruments and Methods in Physics Research Section A: Accelerators, Spectrometers, Detectors and Associated Equipment* pp. 101–105 (2003).
15. E. Saldin, E. Schneidmiller, and M. Yurkov, "Statistical properties of the radiation from vuv fel at desy operating at 30nm wavelength in the femtosecond regime," Nuclear Instruments and Methods in Physics Research Section A: Accelerators, Spectrometers, Detectors and Associated Equipment **562**(1), 472–486 (2006).
16. E. Schneidmiller and M. Yurkov, "Application of Statistical Methods for Measurements of the Coherence Properties of the Radiation from SASE FEL," in *7th International Particle Accelerator Conference*, (2016), p. MOPOW013.
17. C. Behrens, N. Gerasimova, C. Gerth, B. Schmidt, E. Schneidmiller, S. Serkez, S. Wesch, and M. Yurkov, "Constraints on photon pulse duration from longitudinal electron beamdiagnostics at a soft x-ray free-electron laser," Physical Review Special Topics - Accelerators and Beams **15**(3), 030707 (2012).
18. A. Singer, F. Sorgenfrei, A. P. Mancuso, N. Gerasimova, O. M. Yefanov, J. Gulden, T. Gorniak, T. Senkbeil, A. Sakdinawat, Y. Liu, D. Attwood, S. Dziarzhytski, D. D. Mai, R. Treusch, E. Weckert, T. Salditt, A. Rosenhahn, W. Wurth, and I. A. Vartanyants, "Spatial and temporal coherence properties of single free-electron laser pulses," Opt. Express **20**(16), 17480–17495 (2012).
19. A. A. Lutman, Y. Ding, Y. Feng, Z. Huang, M. Messerschmidt, J. Wu, and J. Krzywinski, "Femtosecond x-ray free electron laser pulse duration measurement from spectral correlation function," Phys. Rev. Spec. Top.–Accel. Beams **15**(3), 030705 (2012).

Optics EXPRESS

20. Y. Inubushi, K. Tono, T. Togashi, T. Sato, T. Hatsul, T. Kameshima, K. Togawa, T. Hara, T. Tanaka, H. Tanaka, T. Ishikawa, and M. Yabashi, "Determination of the pulse duration of an x-ray free electron laser using highly resolved single-shot spectra," Phys. Rev. Lett. **109**(14), 144801 (2012).
21. R. Engel, S. Düsterer, G. Brenner, and U. Teubner, "Quasi-real-time photon pulse duration measurement by analysis of FEL radiation spectra," J. Synchrotron Radiat. **23**(1), 118–122 (2016).
22. U. Fruehling, M. Wieland, M. Gensch, T. Gebert, B. Schutte, M. Krikunova, R. Kalms, F. Budzyn, O. Grimm, J. Rossbach, E. Plönjes, and M. Drescher, "Single-shot terahertz-field-driven x-ray streak camera," Nat. Photonics **3**(9), 523–528 (2009).
23. I. Grguras, A. R. Maier, C. Behrens, T. Mazza, T. J. Kelly, P. Radcliffe, S. Dusterer, A. K. Kazansky, N. M. Kabachnik, Th. Tschentscher, J. T. Costello, M. Meyer, M. C. Hoffman, H. Schlarb, and A. L. Cavalieri, "Ultrafast x-ray pulse characterization at free-electron lasers," Nat. Photonics **6**(12), 852–857 (2012).
24. R. Ivanov, J. Liu, G. Brenner, M. Brachmanski, and S. Düsterer, "FLASH free-electron laser single-shot temporal diagnostic: terahertz-field-driven streaking," J. Synchrotron Radiat. **25**(1), 26–31 (2018).
25. E. Saldin, E. Schneidmiller, and M. Yurkov, "Fast: a three-dimensional time-dependent fel simulation code," Nuclear Instruments and Methods in Physics Research Section A: Accelerators, Spectrometers, Detectors and Associated Equipment **429**(1-3), 233–237 (1999).
26. T. Pfeifer, Y. Jiang, S. Düsterer, R. Moshammer, and J. Ullrich, "Partial-coherence method to model experimental free-electron laser pulse statistics," Opt. Lett. **35**(20), 3441–3443 (2010).
27. R. Bonifacio, C. Pellegrini, and L. M. Narducci, "Collective instabilities and high-gain regime in a free electron laser," Opt. Commun. **50**(6), 373–378 (1984).
28. L. Mandel and E. Wolf, "The measures of bandwidth and coherence time in optics," Proceedings of the Physical Society **80**(4), 894–897 (1962).
29. R. Bonifacio, F. Casagrande, and L. De Salvo Souza, "Collective variable description of a free-electron laser," Phys. Rev. A **33**(4), 2836–2839 (1986).
30. E. Saldin, E. Schneidmiller, and M. Yurkov, "Statistical properties of radiation from vuv and x-ray free electron laser," Opt. Commun. **148**(4-6), 383–403 (1998).
31. S. Krinsky and R. L. Gluckstern, "Analysis of statistical correlations and intensity spiking in the self-amplified spontaneous-emission free-electron laser," Phys. Rev. Spec. Top.–Accel. Beams **6**(5), 050701 (2003).
32. M. Martins, M. Wellhöfer, J. Hoeft, W. Wurth, J. Feldhaus, and R. Follath, "Monochromator beamline for flash," Rev. Sci. Instrum. **77**(11), 115108 (2006).
33. N. Gerasimova, S. Dziarzhytski, and J. Feldhaus, "The monochromator beamline at flash: Performance, capabilities and upgrade plans," J. Mod. Opt. **58**(16), 1480–1485 (2011).
34. H. Redlin, A. Al-Shemmary, A. Azima, N. Stojanovic, F. Tavella, I. Will, and S. Dústerer, "The flash pump–probe laser system: Setup, characterization and optical beamlines," Nuclear Instruments and Methods in Physics Research Section A: Accelerators, Spectrometers, Detectors and Associated Equipment **635**(1), S88–S93 (2011).
35. S. Schulz, I. Grguras, C. Behrens, H. Bromberger, J.T. Costello, M.K. Czwalinna, M. Felber, M.C. Hoffman, M. Ilchen, H.Y. Liu, T. Mazza, M. Meyer, S. Pfeiffer, P. Predki, S. Schefer, C. Schmidt, U. Wegner, H. Schlarb, and A.L. Cavalieri, "Femtosecond all-optical synchronization of an x-ray free-electron laser," Nat. Commun. **6**(1), 5938 (2015).
36. R. Ivanov, I. J. B. Macias, J. Liu, G. Brenner, J. Roensch-Schulenburg, G. Kurdi, U. Frühling, K. Wenig, S. Walther, A. Dimitriou, M. Drescher, I. P. Sazhina, A. K. Kazansky, N. M. Kabachnik, and S. Dústerer, "Single-shot temporal characterization of XUV pulses with duration from ~10 fs to ~350 fs at FLASH," J. Phys. B: At., Mol. Opt. Phys. **53**(18), 184004 (2020).
37. S. Roling, "Temporal and spatial coherence properties of free-electron-laser pulses in the extreme ultraviolet regime," Physical Review Special Topics - Accelerators and Beams **14**(8), 080701 (2011).